# Magnetic circular dichroism in the soft-x-ray absorption spectra of Mn-based magnetic intermetallic compounds

A. Kimura,* S. Suga, T. Shishidou, S. Imada, and T. Muro
*Department of Material Physics, Faculty of Engineering Science, Osaka University, Toyonaka, Osaka 560, Japan*

S. Y. Park and T. Miyahara
*Photon Factory, National Laboratory for High Energy Physics, Oho 1-1, Tsukuba, Ibaraki 305, Japan*

T. Kaneko
*The Research Institute for Iron, Steel and Other Metals, Tohoku University, Katahira, Sendai, Miyagi 980, Japan*

T. Kanomata
*Department of Applied Physics, Faculty of Technology, Tohoku Gakuin University, Tagajo, Miyagi 985, Japan*

We have investigated the magnetic electronic structures of PtMnSb, NiMnSb, $Ni_2MnSb$,MnSb, MnAlGe, and $Mn_2Sb$ by soft-x-ray absorption spectroscopy (XAS) and magnetic circular dichroism (MCD) measurements in the Mn $2p$ core absorption region. Different degrees of the electron itinerancy of the Mn $3d$ states are discussed. The large orbital angular momentum of the Mn $3d$ electrons is revealed for MnSb by the MCD spectrum. In addition, the XAS and MCD spectra are measured in the Sb $3d$, Ni $2p$, and Pt $4f$ core excitation regions. An induced magnetic moment of Sb valence orbitals with the spin antiparallel to that of Mn is clearly indicated for NiMnSb and $Mn_2Sb$. [S0163-1829(97)07734-5]

## I. INTRODUCTION

Several Mn-based alloys show very interesting properties in terms of complicated magnetic phase transitions, strong magneto-optical effects, and strong magnetic anisotropies, and so on. Among them, PtMnSb and NiMnSb have the $C1_b$ crystal structure and show the ferromagnetic phase with a $T_c$ of 575 and 730 K, respectively.[1] $Ni_2MnSb$ is also a ferromagnetic alloy with the $L2_1$ crystal structure. PtMnSb, NiMnSb, and $Ni_2MnSb$ are generally called Heusler alloys. In PtMnSb and NiMnSb, the observed magnetic moments of the Mn atom are about $4\mu_B$, whereas that of the $Ni_2MnSb$ is $3.27\mu_B$.[1] It is reported for PtMnSb that the polar Kerr effect is unusually high. For an incident light with a wavelength of 720 nm (~1.7 eV), a rotation up to $-1.27°$ is found.[2] This is the highest rotation ever found in a metallic material at room temperature. NiMnSb shows a smaller magnitude of the Kerr rotation angle compared with that of PtMnSb.[2]

Ferromagnetic MnSb and MnBi have the NiAs-type crystal structure and are well known to show the strong uniaxial magnetic anisotropy. At high temperatures, the $c$ axis is the easy direction of magnetization in both alloys. In MnSb the easy magnetization direction changes into the $a$-$b$ plane at 510 K. On the other hand, the easy magnetization axis of MnBi gradually deviates from the $c$ axis below 142 K, and changes into the $a$-$b$ plane at 90 K.[3,4]

In contrast with this, $Mn_2Sb$ and MnAlGe have the $Cu_2Sb$-type crystal structure. $Mn_2Sb$ has a ferrimagnetic structure with a $T_c$ of 550 K. The inequivalent Mn sites, Mn(I) and Mn(II), bear different magnetic moments below $T_c$ with an antiparallel alignment.[5] On the other hand, MnAlGe is a simple ferromagnet with $T_c$ of 518 K, since the

nonmagnetic Al atoms preferentially occupy the II site, whereas Mn atoms occupy only the I site.[5] A spin reorientation phenomenon is also observed in $Mn_2Sb$. The neutron-diffraction studies have revealed that there is a spin-flop transition at $T_{sf} = 240$ K, where the easy magnetization direction is aligned parallel and perpendicular to the $c$ axis above and below this temperature.[5]

Band calculations have been intensively carried out for these Mn alloys. De Groot et al.[6] performed a self-consistent and scalar-relativistic band calculation on PtMnSb and NiMnSb and discussed the magneto-optical Kerr effect (MOKE) by considering the unusual features of the spin-polarized band structures. For example, the majority-spin band crosses the Fermi level ($E_F$), whereas the minority-spin band shows semiconducting characters. They proposed that the incomplete cancellation of optical transitions by the different helicity lights induced the large MOKE in PtMnSb, whereas the small MOKE of NiMnSb was due to the higher location of the Fermi energy resulting in larger cancellation. Later, Wijingaard, Haas, and de Groot[7] have reinvestigated the influence of the scalar-relativistic effects on the electronic structures of PtMnSb and NiMnSb and suggested that this effect is responsible for the large difference in MOKE (between PtMnSb and NiMnSb) even without considering the spin-orbit interaction. Recently, Oppeneer et al.[8] have calculated the Kerr rotation and ellipticity spectra of PtMnSb from the first-principles band calculation including the spin-orbit interaction and concluded that the spin-orbit coupling of Pt as well as that of Sb play important roles in the large Kerr rotation in PtMnSb.

Although the localized spin character is well known in several Heusler alloys, their electronic structures have often
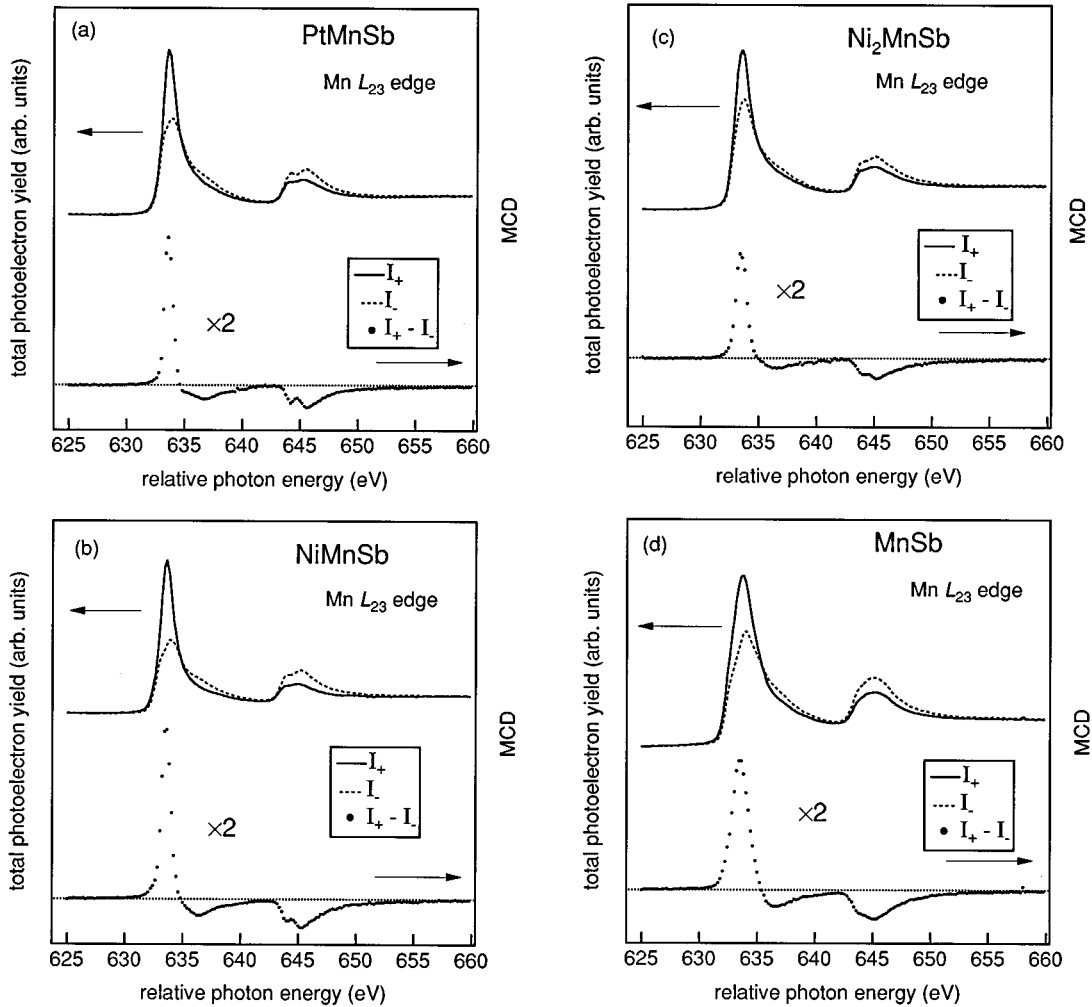
FIG. 1. Mn $2p$ XAS and MCD spectra of (a) PtMnSb, (b) NiMnSb, (c) Ni$_2$MnSb, (d) MnSb, (e) Mn$_2$Sb, and (f) MnAlGe. The solid curve (dashed curve) indicates the absorption intensity with the directions between the magnetization and the photon spin parallel (antiparallel) as denoted by $I_+$ ($I_-$). The dots show the MCD spectrum.

been understood in terms of the one-electron band pictures. Kübler, Williams, and Sommers[9] have suggested for the $L2_1$-type Heusler alloys ($X_2$MnY) that the Mn $3d$ majority-spin states are almost occupied and their wide bandwidths indicate that they are just as delocalized as the $d$ electrons of Co, Ni, Cu, or Pd. On the contrary, the Mn $3d$ minority-spin states are nearly empty.

As for the electronic structure of MnSb, several models have been proposed. In the ionic model proposed by Goodenough, the Mn atom has essentially four $d$ electrons.[10] On the other hand, Chen *et al.*[11] and Allen and Mikkelsen[12] have suggested an alloylike band model (without considering hybridization) in which the observed magnetic moment of $3.5\mu_B$ per Mn atom is explained. Both ionic and alloylike models imply a high Mn $3d$ density of states (DOS) at the Fermi level in contrast to the small contribution in the electronic specific heat.[11] Coehoorn, Haas, and de Groot have calculated the spin-polarized band structure of MnSb by using the self-consistent augmented-spherical-wave (ASW) method and shown that an exchange splitting of the Mn $3d$ band is about 3.5 eV.[13] Due to the strongly covalent Mn-Sb interaction, the magnetic moment per Mn atom is $3.3\mu_B$, consistent with the experimental result.

We have measured the MCD spectra in the Mn and Sb core excitation regions, in order to clarify the spin-dependent electronic structures of these alloys. Much information is obtained for such phenomena as the hybridization between the Mn and Sb atoms, magnetic anisotropy and the orbital contribution to the magnetic moments. In addition, the electronic states of the Ni $3d$ orbital are discussed through the MCD spectra in the Ni $2p$ core excitation region of NiMnSb and Ni$_2$MnSb.

## II. EXPERIMENTAL

The Mn $2p$, Ni $2p$, and Sb $3d$ x-ray-absorption spectroscopy (XAS) and magnetic circular dichroism (MCD) spectra were measured at the NE1B beamline of the TRISTAN Accumulation Ring in National Laboratory for High Energy Physics (KEK). Circularly polarized light was supplied from a helical undulator, with which almost complete polarization was obtained at the peak of the first-harmonic radiation.

The XAS spectra were measured by means of the total photoelectron yield by directly detecting the sample current with changing the photon energy ($h\nu$). It is widely known that the total photoelectron yield well represents the absorp-
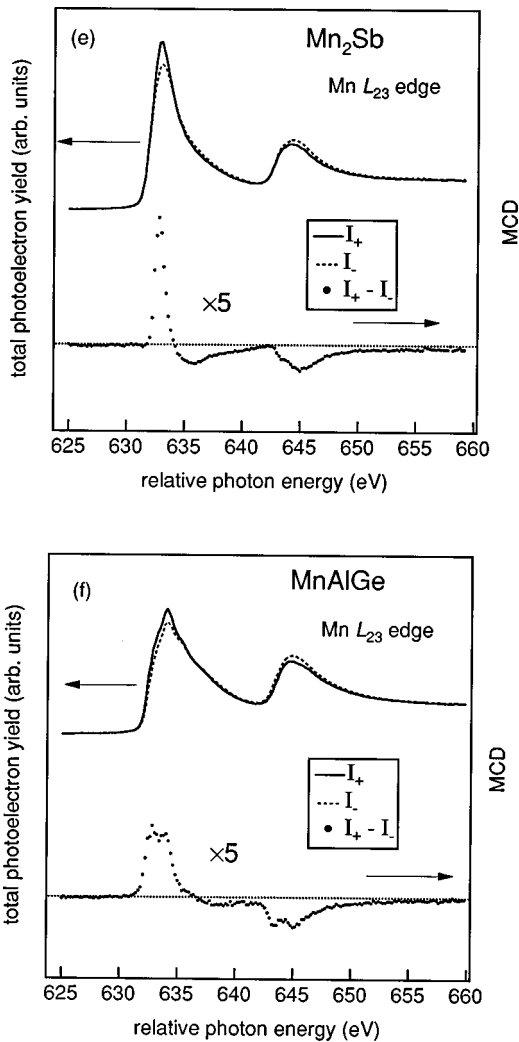
FIG. 1. (*Continued*).

tion in the core excitation region. The magnetic field of about 1.1 T was applied with using the permanent magnet made of the Nd-Fe-B alloy. The MCD spectra were taken for a particular helicity of light by reversing the applied magnetic field at each $h\nu$. In the present paper, the MCD spectrum is defined as $I_+ - I_-$, where $I_+$ and $I_-$ represent the absorption intensity with the direction of the magnetization (which is opposite to the majority spin) being parallel and antiparallel to the photon spin (helicity), respectively.

Clean surfaces were obtained by *in situ* diamond-file scraping of the sample under the ultrahigh vacuum condition ($<1\times10^{-9}$ Torr). The cleanliness of the sample surface was first checked by the disappearance of the typical structure related to the Mn oxides. Namely, the $3d$ electrons of the present Mn alloys are rather itinerant and their Mn $2p$ and $3p$ XAS spectra are somewhat broader than those of the insulating Mn oxides. We could also check the degree of contamination from the magnitude of the MCD signal, because its amplitude grew and finally saturated when the sample surface became clean enough. We thought that the unscraped or contaminated surface was covered with the antiferromagnetic or paramagnetic compounds such as Mn oxides, which hardly contributed to the MCD spectrum.

## III. RESULTS

The total photoelectron yield (XAS) and MCD spectra in the Mn $2p$ core ($L_{23}$) excitation regions of several Mn alloys are summarized in Figs. 1(a)–1(f). Clear multiplet structures are found in the Mn $2p$ XAS spectra of PtMnSb, NiMnSb, and Ni$_2$MnSb as shown in Figs. 1(a)–1(c). In these spectra, a sharp peak structure and a doublet structure are observed in the Mn $2p_{3/2}$ and $2p_{1/2}$ core excitation regions, respectively. In addition, some shoulder structure is found on the larger energy side of the $2p_{3/2}$ component in the $I_-$ spectra. Such a shoulder is somewhat weaker in the case of Ni$_2$MnSb. As for the MCD spectra of PtMnSb, NiMnSb, and Ni$_2$MnSb, a prominently positive and a small negative signal are found within the $2p_{3/2}$ core excitation region with increasing $h\nu$ and small negative signals with double-peak structures are recognized in the $2p_{1/2}$ region.

As shown in Fig. 1(d), the Mn $2p$ XAS spectrum of MnSb shows a broader line shape with no clear multiplet structures in both the $2p_{3/2}$ and $2p_{1/2}$ components compared with those of PtMnSb, NiMnSb, and Ni$_2$MnSb. The appreciable tail is recognized toward higher $h\nu$ as in other materials. The MCD spectrum shows the positive and negative signs within the $2p_{3/2}$ region. It is found that the spectral width of the positive MCD signal on the lower energy side of the Mn $2p_{3/2}$ absorption peak is considerably broader than those of the Heusler alloys. The doublet MCD feature in the $2p_{1/2}$ region is much broadened in MnSb.

The Mn $2p$ XAS spectrum of Mn$_2$Sb [Fig. 1(e)] neither shows clear multiplet structures. The intensity of the tail of the $2p_{3/2}$ XAS in the higher-energy region is comparable to that in the spectrum of MnSb. As for the MCD of Mn$_2$Sb one recognizes a clear feature that the spectral width of the positive MCD signal of the $2p_{3/2}$ component is much narrower than that of MnSb and is comparable to those of PtMnSb, NiMnSb, and Ni$_2$MnSb. The $2p_{1/2}$ MCD structure, however, does not show a clear doublet spectral shape compared with the Heusler alloys. Besides, the magnitude of MCD in Mn$_2$Sb is much smaller compared with those of the Heusler alloys.

Both the XAS and MCD spectra of MnAlGe are quite different from these results. First, the XAS spectrum shows much broader and asymmetric line shapes for both $2p_{3/2}$ and $2p_{1/2}$ core excitations as shown in Fig. 1(f). The MCD spectrum is also much different from others as follows: the positive MCD in the lower energy portion of the $2p_{3/2}$ component is quite broad and has some structures. In addition, a clear doublet is observed in the negative MCD of $2p_{1/2}$ component in contrast to its featureless XAS structure.

The XAS and MCD spectra in the Ni $2p$ core ($L_{23}$) excitation region are also measured in NiMnSb and Ni$_2$MnSb. As shown in Figs. 2(a) and 2(b), several faint multiplet structures are found in XAS. As for the MCD spectrum of Ni$_2$MnSb [Fig. 2(b)], it is found that a positive and a negative MCD signal are predominantly observed in the regions of the $2p_{3/2}$ and $2p_{1/2}$ components, respectively. The gross feature of the MCD spectrum of NiMnSb [Fig. 2(a)] is likewise. It is, however, noticed that a small but quite clear structure with the opposite sign to that of the main MCD signal appears at the threshold of the $2p_{3/2}$ absorption peak (and possibly at the $2p_{1/2}$ threshold) as shown by the arrow.
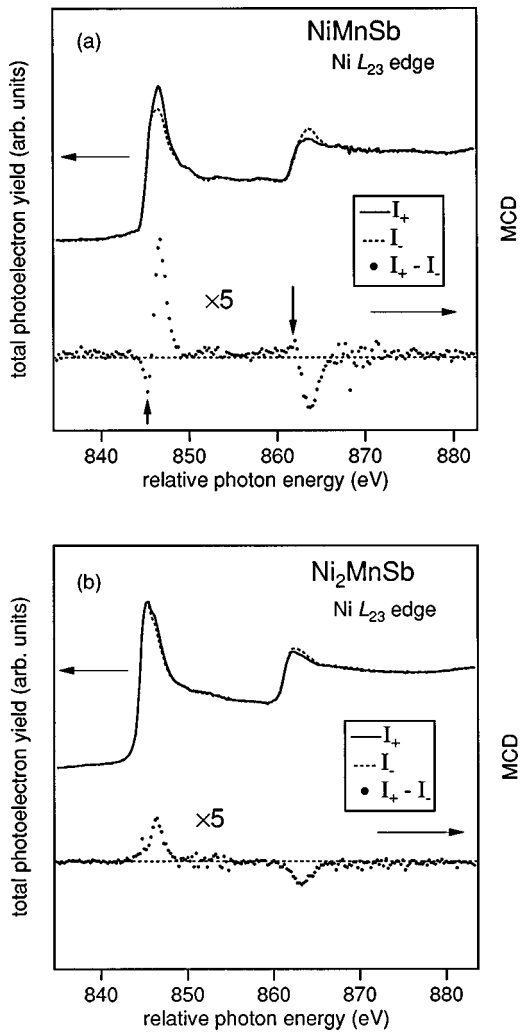
FIG. 2. Ni $2p$ XAS (solid and dashed curves) and MCD spectra (dots) of (a) NiMnSb and (b) Ni$_2$MnSb.



FIG. 3. Sb $3d$ XAS (solid and dashed curves) and MCD spectra (dots) of (a) NiMnSb and (b) Mn$_2$Sb.

Such a feature is not observed in Ni$_2$MnSb. So far, the magnetic moments on the Ni sites for NiMnSb and Ni$_2$MnSb are reported to be almost 0 by the neutron-diffraction studies.[1] On the contrary, the present Ni $2p$ core MCD spectra of NiMnSb and Ni$_2$MnSb indicate that there is a finite magnetic moment on the Ni site which is parallel to that of Mn and the magnetic moment on the Ni atom is larger for NiMnSb than for Ni$_2$MnSb.

Another very important result is the observation of weak but very clear MCD features even in the Sb $3d \rightarrow 5p$ (and $\varepsilon f$) excitation region in NiMnSb and Mn$_2$Sb [Figs. 3(a) and 3(b)]. Similar measurements are not yet done for other Sb compounds. The Sb $3d \rightarrow 5p$ XAS spectrum of these alloys shows the spin-orbit split components, i.e., $3d_{5/2}$ and $3d_{3/2}$ with the energy separation of about 10 eV. The gradual increase of XAS toward higher $h\nu$ is interpreted as due to the delayed onset of the giant absorption due to the Sb $3d \rightarrow \varepsilon f$ transition. Positive and negative MCD signals are observed for the $3d_{5/2}$ and $3d_{3/2}$ main absorption components, in both NiMnSb and Mn$_2$Sb. Such clear MCD spectra strongly indicate the induced magnetic moments on the Sb sites in NiMnSb and Mn$_2$Sb.

Then XAS and MCD spectra taken in the Mn $3p$ core ($M_{23}$) excitation region of several Mn alloys are given in
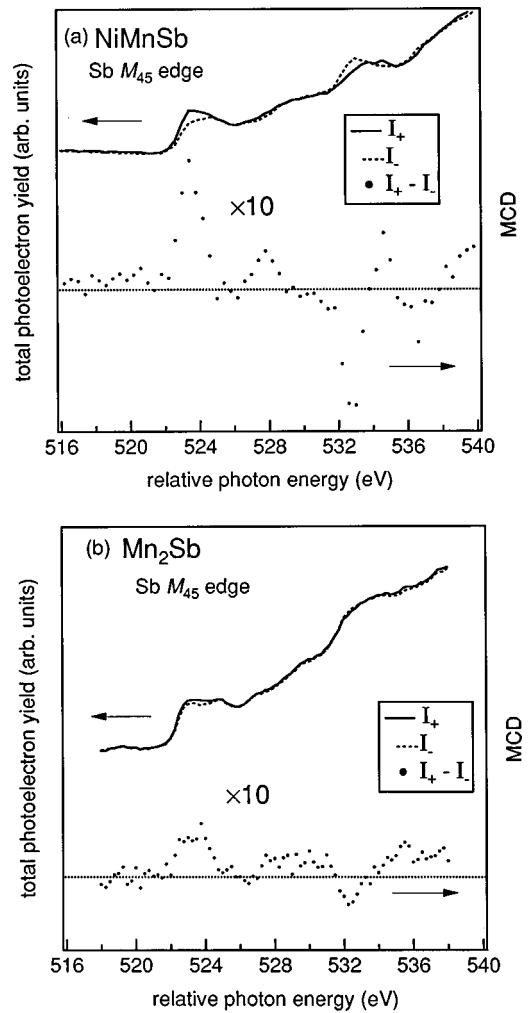
Figs. 4(a)–4(d). All the XAS spectra show asymmetric line shapes with remarkable tails. The intensity of the tail increases sometimes toward higher $h\nu$. The XAS spectra of PtMnSb, NiMnSb show similar spectral line shapes except for the broad hump located around $h\nu = 60$ eV in PtMnSb [Fig. 4(a)]. Similarities are also recognized in the MCD spectra of PtMnSb and NiMnSb, where normal MCD signals with the positive-negative peaks are observed. The positive MCD signal located at $h\nu = 58$ eV in the spectrum of PtMnSb is possibly caused by the $5p_{3/2}$ ($O_3$) excitation of Pt which has the moment parallel to that of the Mn $3d$ state. As shown in Fig. 4(c) for MnSb, the onset of the MCD is located at lower $h\nu$ compared with the Heusler alloys. Consequently, the width of the positive MCD band is broader in MnSb than in the Heusler alloys.

It is recognized in Fig. 4(d) that the $M_{23}$ XAS spectrum of MnAlGe shows a prominent dip structure around $h\nu = 48$ eV followed by a quite broad peak, whereas the absorption spectra of other materials have peak structures around $h\nu = 52$ eV with no noticeable dip in the smaller $h\nu$ region. This dip feature was already observed in the constant initial state spectra for the Mn $3d$ photoemission[14] in MnAlGe. The $M_{23}$ MCD spectrum has clear multiplet structures with predominantly positive sign over the whole region. This result is in strong contrast to the Mn $2p$ ($L_{23}$) MCD.
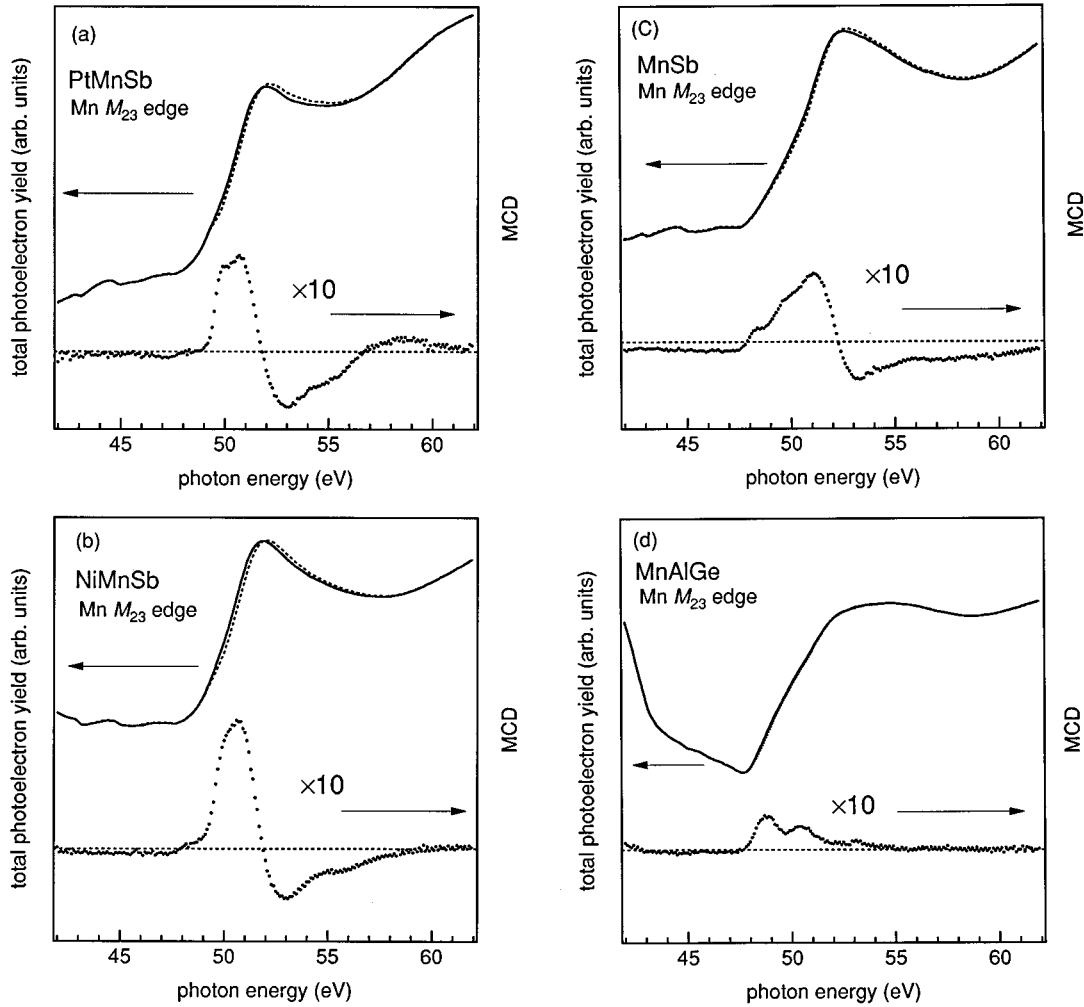
FIG. 4. Mn $3p$ XAS and MCD spectra of (a) PtMnSb, (b) NiMnSb, (c) MnSb, and (d) MnAlGe.

## IV. DISCUSSION

### A. Spectral line shapes

First, the degree of the electron itinerancy will be discussed from the view point of the line shapes of the Mn $2p$ XAS and MCD spectra. The spectra will be compared with atomic multiplets and band-calculation results.

#### 1. Heusler alloys

It has been shown that the Mn $2p$ XAS spectra of PtMnSb, NiMnSb, and $Ni_2MnSb$ have rather common features. Such features as for the $2p_{3/2}$ component, a sharp XAS peak with a remarkable tail toward higher $h\nu$ and a clear doublet in the $2p_{1/2}$ component, are also observed in the Mn $2p$ XAS spectra of gas-phase Mn and impurity Mn diluted in noble-metal hosts.[15] In Fig. 5 are reproduced the Mn $2p$ XAS multiplet spectra calculated with assuming a magnetized high-spin Mn $3d^5$ configuration in the ground state. (The calculation for the $3d^6$ ground state is given in Fig. 6 for comparison.) The calculation is done for the plus and minus helicity lights with the same quantization axis as the spin. Table I summarizes the $d$-$d$ and $d$-core Slater integrals and the spin-orbit constants for the $3d$ and core levels used in the calculation. The Slater integrals are obtained by reducing

the Hartree-Fock values by the factor 0.8. The calculated XAS and MCD spectra in Fig. 5 qualitatively reproduce the essential features of the experimental spectra of the Heusler alloys.

The calculated Mn $3p$ MCD spectrum for the $3d^5$ configuration in the ground state shows a simple dispersive structure (Fig. 7) which is qualitatively consistent with the experimental spectra of PtMnSb, NiMnSb, and $Ni_2MnSb$. However, the broad and asymmetric line shape of the observed $3p$ core absorption spectra with a tails, in particular, toward higher $h\nu$ is not well reproduced in the calculation. Such an asymmetry is probably caused by the interference effect which is not included in the calculation. In fact, the discrete excitations, $3p^6 3d^n \rightarrow 3p^5 3d^{n+1}$ followed by the super Coster-Krönig decay channel given by $3p^5 3d^{n+1} \rightarrow 3p^6 3d^{n-1} \varepsilon 1$ is coupled with the continuum transitions, $3p^6 3d^n \rightarrow 3p^6 3d^{n-1} \varepsilon 1$. A Fano-type interference thus induced provides the asymmetry even in the spectrum of gas phase Mn,[16] in which clear multiplet structures exist around the prethreshold region. The gross feature of the XAS spectral line shape of pure metallic Mn is similar to that of the atomic Mn,[16] but shows no multiplet structure around the prethreshold region.

When we try to interpret the spectra on the basis of the band model, we should refer to the band calculation.[17,18] The
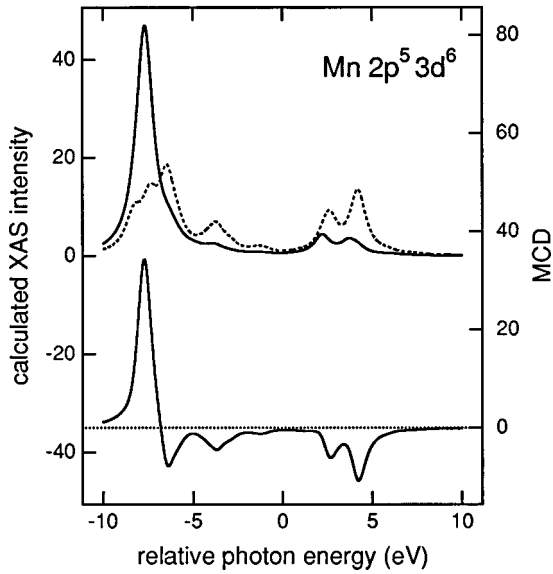
FIG. 5. Calculated Mn $2p$ XAS and MCD spectra for the Mn $2p^6 3d^5 \rightarrow 2p^5 3d^6$ transition, where the solid (dashed) curve denotes the $I_+$ ($I_-$) spectrum. Lower part: calculated MCD spectrum ($I_+ - I_-$) shown by the solid curve. The Lorentzian convolution of $2\Gamma = 1.0$ eV is used.

spin-polarized DOS of PtMnSb and NiMnSb (Refs. 17, 18) show a large intra-atomic exchange splitting of the Mn $3d$ states resulting in the almost occupied (unoccupied) majority- (minority-) spin state. The obtained values of the Mn $3d$ electron number ($n_d$) and the magnetic moment ($\mu_d$) of the Mn $3d$ states are $n_d = 5.36$ and $3.78\mu_B$/Mn atom in PtMnSb and $n_d = 5.38$ and $3.62\mu_B$/Mn in NiMnSb.[17] Since the Ni $3d$ or Pt $5d$ states are considered to be almost occupied for both spin directions, the hybridization between the minority-spin Mn $3d$ and the Ni $3d$ or Pt $5d$ states is not so strong. Furthermore the hybridization between the neighboring Mn atoms is weak due to the large atomic distance of about 4 Å in these Heusler materials. Therefore the bandwidth of the unoccupied minority-spin state is considered to be rather narrow in NiMnSb and PtMnSb. Actually, the bandwidth of the minority-spin Mn $3d$ states is calculated to be about 2.5 eV for PtMnSb and NiMnSb.[18] This situation seems to be reflected in the narrow spectral shape of the Mn $2p$ XAS.

### 2. MnSb

The broader spectral shapes of the Mn $2p$ XAS spectrum of MnSb with no clear multiplets cannot be simply reproduced by the $2p^5 3d^6$ multiplet calculation. It is widely known that the increase of the itinerancy of the Mn $3d$ electrons in metallic Mn systems provides broader spectral shapes. If the bandwidth of the Mn $3d$ states becomes greater than the energy splitting between the different electron configurations in the ground state, the XAS final state is expected to involve more than two electron configurations providing broader line shape. This was suggested by Thole *et al.*[19] In addition, the broader Mn $3p$ MCD spectrum of MnSb is consistent with its broader feature of the Mn $2p$ MCD.

The band calculation shows that the hybridization between the neighboring Mn is important in MnSb because of
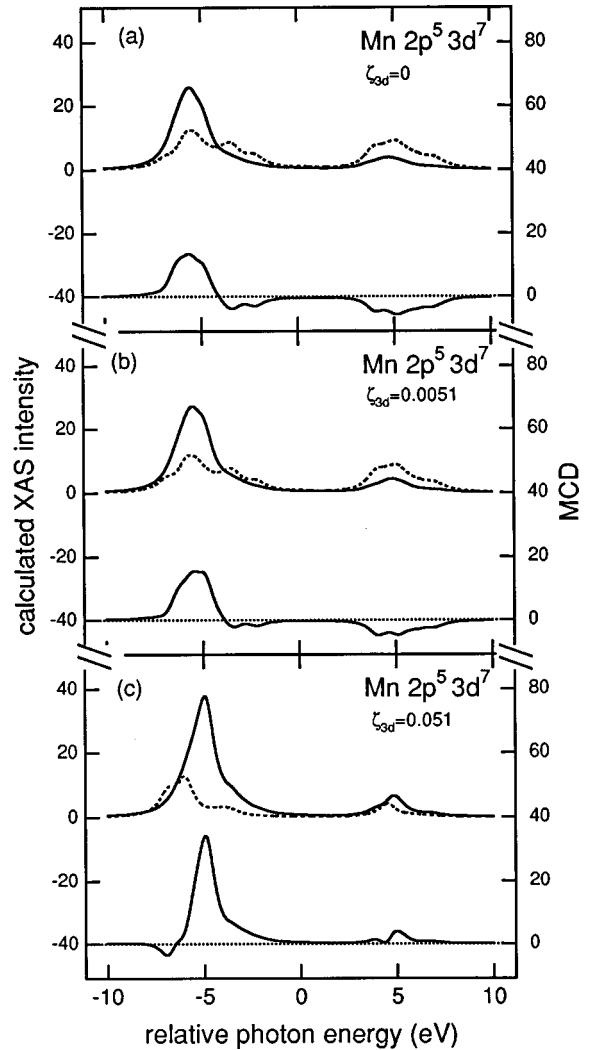


FIG. 6. Calculated Mn $2p$ XAS and MCD spectra for the Mn $2p^6 3d^6 \rightarrow 2p^5 3d^7$ transition without considering the crystal-field terms of the Mn $3d$ state for the spin-orbit interaction of the Mn $3d$ state set to (a) 0, (b) 10% of Hartree-Fock (HF), and (c) full HF values. The Lorentzian convolution of $2\Gamma = 1.0$ eV is used.

the shorter Mn-Mn distance ($\sim 2.87$ Å).[20] The calculated bandwidth of MnSb is about 5 eV for both of the minority- and majority-spin states which is about two times broader than those of the Heusler alloys for the minority-spin states.[13] The calculated electron number and the magnetic moment of the Mn $3d$ state are $n_d = 5.59$ and $3.24\mu_B$/Mn in MnSb, which are larger and smaller, respectively, than those of the Heusler alloys, indicating the more itinerant character of the Mn $3d$ electrons in MnSb. The deviation from the half-filled scheme in MnSb can qualitatively explain the spectral shapes of the Mn $2p$ XAS and MCD spectra as discussed above.

### 3. Mn$_2$Sb

For understanding the Mn $2p$ XAS and MCD spectra of ferrimagnetic Mn$_2$Sb, the inequivalent contributions of the two Mn sites should be taken into account. The band calculation shows that the itinerancy of Mn(I) $3d$ state is stronger than that of Mn(II) $3d$ state.[21] The calculated electron numbers and the magnetic moments of the Mn $3d$ state are $n_d$
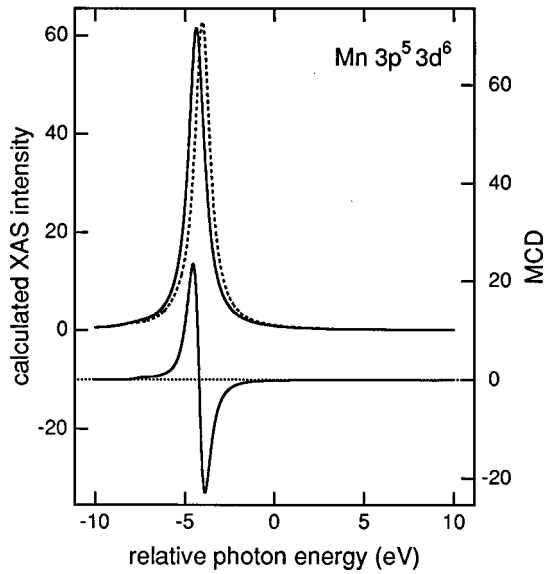
FIG. 7. Calculated Mn $3p$ XAS and MCD spectra for the Mn $3p^6 3d^5 \rightarrow 3p^5 3d^6$ transition, where the solid (dashed) curve denotes the $I_+$ ($I_-$) spectrum. Lower part: calculated MCD spectrum ($I_+ - I_-$) shown by the solid curve. The Lorentzian convolution of $2\Gamma = 1.0$ eV is used.

$=5.71$ and $2.30 \mu_B/$Mn for Mn(I) and $n_d = 5.36$ and $3.60 \mu_B/$Mn for Mn(II) in ferrimagnetic state.[21] The calculated bandwidth of the Mn(I) $3d$ state is around 6 eV which is broader than that of the Mn(II) $3d$ state ($\sim 5$ eV) indicating more itinerant character of the Mn(I) $3d$ electron.[21] Since the quantization axis is defined along the direction of the total magnetic moment, the Mn(II) $3d$ majority spin in Mn$_2$Sb is antiparallel to the magnetic field (down spin is the majority spin). The Mn(I) $3d$ majority spin, being antiparallel to the majority Mn(II) spin in the ferrimagnetic phase, is parallel to the magnetic field (up spin). So the signs of the MCD signals from the Mn(I) should be opposite to that of the Mn(II). Actually, the observed Mn $2p$ MCD spectrum of Mn$_2$Sb is rather similar to those of the Heusler alloys except for the slightly broader spectral shape of the double peak observed in the $2p_{1/2}$ region. This result indicates that the MCD spectrum derived from the Mn(II) site predominates the total MCD spectrum in Mn$_2$Sb. The magnitude of MCD is, however, smaller than those of the Heusler alloys, probably due to the cancellation between the Mn(I) and Mn(II) contributions.

### 4. MnAlGe

The strong itinerancy of the Mn $3d$ electrons in MnAlGe has been pointed out already by photoemission, inverse photoemission, and band-calculation studies.[14,22–24] Although it is considered to be important to include the hybridization effect in the interpretation of the XAS and MCD spectra of MnAlGe, we again compare the Mn $2p$ XAS and MCD spectra with the results of atomic multiplet calculation for the $2p^5 3d^{n+1}$ configurations for simplicity. It is soon noticed that their line shapes are better explained in terms of the atomic multiplets for the $2p^5 3d^7$ configuration than for the $2p^5 3d^6$ configuration. The crystal-field ($10Dq$) and the spin-orbit interaction of the Mn $3d$ state are neglected in Fig.
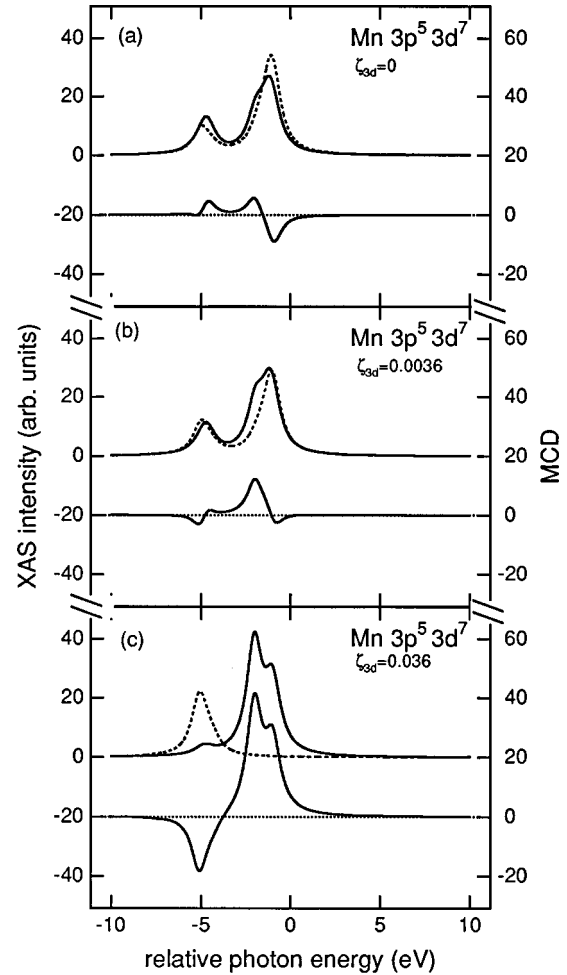


FIG. 8. Calculated Mn $3p$ XAS and MCD spectra for the Mn $3p^6 3d^6 \rightarrow 3p^5 3d^7$ transition without considering the crystal-field term. The conditions for (a), (b), and (c) are the same as in Fig. 6.

6(a), where broad and highly asymmetric line shapes are recognized for the $2p_{3/2}$ component in the $I_+$ and $I_-$ spectra compared with the corresponding spectra for the Mn $2p^5 3d^6$ in Fig. 5. The calculated MCD spectrum has revealed a positive and broad spectral line shape in the lower energy region of the $2p_{3/2}$ component. Still the double-peak MCD structure in the $2p_{1/2}$ region is seen in this calculation. Thus such characteristic features of the calculated XAS and MCD spectra for the $2p^5 3d^7$ system can qualitatively explain the experimental spectra of both MnAlGe (the spectra of MnSb can be likewise explained).

For further examining the spectral shapes, the results calculated with considering the spin-orbit interaction are shown in Figs. 6(b) and 6(c). The spin-orbit interaction strength is set to the full Hartree-Fock (HF) value in Fig. 6(c) and to 10% of it in Fig. 6(b). The spectrum with 10% of the HF spin-orbit interaction is very similar to that without spin-orbit term. If the HF spin-orbit interaction is fully included in the calculation, the spectral shapes drastically change in both XAS and MCD spectra as shown in Fig. 6(c). The spectral weight of $I_-$ is shifted to lower energies than that of $I_+$ component resulting in the sign reversal of the MCD signal within the $2p_{3/2}$ region. The calculated results (c) are in strong contrast to the case (a) without the spin-orbit term and

TABLE I. The Slater integrals and the spin-orbit constants (in units of eV). The Slater integrals are obtained by reducing the Hartree-Fock values by the factor 0.8.

| | 3d-3d | | 3d-core | | | | |
| | $F^2$ | $F^4$ | $F^2$ | $G^1$ | $G^3$ | $\zeta_{3d}$ | $\zeta_{core}$ |
|---|---|---|---|---|---|---|---|
| $3d^5$ | 8.295 | 5.158 | | | | 0.041 | |
| $3d^6$ | 7.304 | 4.502 | | | | 0.035 | |
| $2p^53d^6$ | 8.966 | 5.581 | 5.177 | 3.904 | 2.198 | 0.058 | 6.595 |
| $2p^53d^7$ | 8.022 | 4.954 | 4.635 | 3.445 | 1.938 | 0.051 | 6.598 |
| $3p^53d^6$ | 8.381 | 5.214 | 9.322 | 11.592 | 7.006 | 0.041 | 0.761 |
| $3p^53d^7$ | 7.464 | 4.606 | 8.641 | 10.743 | 6.441 | 0.036 | 0.746 |

cannot explain the experimental spectra of MnAlGe. It is thus understood that the electron occupation number of the Mn $3d$ states in the ground state is closer to 6 and the spin-orbit interaction of the Mn $3d$ state is unimportant in MnAlGe.

On the other hand, the Mn $3p$ MCD spectrum of MnAlGe [Fig. 4(d)] with the predominantly positive MCD signal over a wide energy range is quite unusual compared with the Mn $2p$ MCD in Fig. 1(f). In the case of the Mn $2p$ MCD, the positive and negative signals corresponding to the $2p_{3/2}$ and $2p_{1/2}$ $h\nu$ components are comparable, leading to an almost negligible amount of the Mn $3d$ orbital angular momentum according to a sum rule[25] as explained later. This apparent discrepancy can be reconciled by considering the much smaller spin-orbit splitting in the Mn $3p$ state resulting in the appreciable cancellation between the positive and negative MCD signals associated with the $3p_{3/2}$ and $3p_{1/2}$ core excitations. Critical balance between the Mn $3p$ and $3d$ spin-orbit splittings, intra-atomic electrostatic interactions, crystal-field splitting, $3d$ bandwidth, hybridization and so on in each individual material may be determining the real XAS and MCD line shape. In order to demonstrate such changes of the spectral line shapes with different magnitude of the Mn $3d$ spin-orbit interaction, we have calculated the Mn $3p$ spectra of $3p^53d^7$ final state in Figs. 8(a), 8(b), and 8(c). The calculated Mn $3p$ MCD spectrum without spin-orbit term (a) shows positive-negative signs with increasing the photon energy, whereas the spectrum with 0.1×HF value of the spin-orbit interaction shows mainly positive structure with very

small negative structures at lower and higher photon energies. Such a remarkable change seen in the Mn $3p$ spectra is in strong contrast to the case of the Mn $2p$ spectra and is considered to be due to the smaller spin-orbit splitting of the Mn $3p$ core hole than that of the Mn $2p$ core state. The MCD spectrum with the full HF value of the Mn $3d$ spin-orbit interaction shows much different line shape, which is negative and positive at lower and higher photon energies, respectively. Our experimental Mn $3p$ MCD spectrum of MnAlGe is qualitatively consistent with the calculated result with small but finite spin-orbit interaction of the Mn $3d$ state in that they show mainly positive signs. The disagreement of the line shapes between theoretical and experimental XAS spectra may be due to the neglect of the Fano-type interference effect in the calculation.

The occupation number of the Mn $3d$ state in MnAlGe is not known. In MnAlGe, Mn atoms occupy only the I site and the electronic state is thought to be not so much modified from that of Mn(I) in $Mn_2Sb$, because the interaction between the Mn(I) and Mn(II) sites in $Mn_2Sb$ is weak due to the antiparallel spin configuration. Therefore, the occupation number is expected to be comparable to that of Mn(I) in $Mn_2Sb$ which is close to 5.7.

### B. Orbital angular momentum

Here, we discuss the orbital angular momentum ($\langle L_z \rangle$) of the $3d$ state. Information about the orbital angular momentum can be obtained by using magnetic sum rules[25] for the
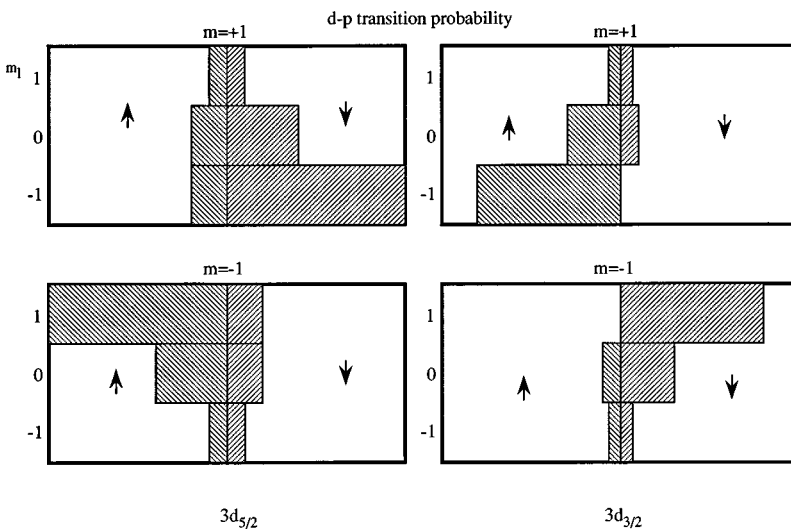


FIG. 9. $d \rightarrow p$ transition probability for the $d_{5/2}$ and $d_{3/2}$ core excitations with the plus- ($\mu = m_d - m_p = +1$) and minus-helicity ($\mu = -1$) light.
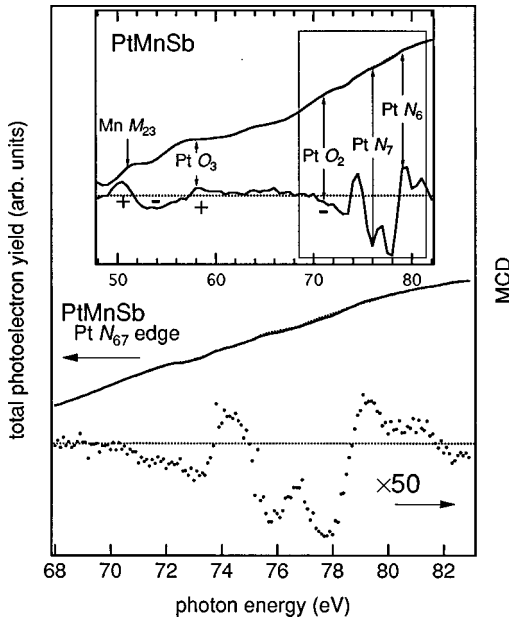
FIG. 10. Pt $4f$ XAS and MCD spectrum of PtMnSb. The inset (upper part) shows the XAS and MCD spectra in the photon energy range from 48 to 82 eV.

Mn $2p$ MCD. For PtMnSb, NiMnSb, and Ni$_2$MnSb, the estimated value of $\langle Lz \rangle / \langle Sz \rangle$ is less than 0.05, whereas it is estimated to be 0.171($\pm$0.002) for MnSb, if the contribution of the magnetic dipole moment is neglected. Besides, the $\langle Lz \rangle / \langle Sz \rangle$ is almost zero for MnAlGe. It is natural that PtMnSb and NiMnSb have quite small orbital angular momentum because of the almost occupied majority-spin state of the Mn $3d$ state as discussed above. On the contrary, deviation from this condition and unbalanced occupation of the magnetic sublevels can induce $\langle Lz \rangle$.[26] The large orbital angular momentum of MnSb suggests an appreciable deviation from the half-filled configuration of the Mn $3d$ state. Here, the estimated value of the $\langle Lz \rangle$ in MnSb has the same sign (negative) as that of the $\langle Sz \rangle$. According to the Hund's rule, this result indicates the more-than-half-filled character of the Mn $3d$ state in MnSb. This is consistent not only with the band calculation but also with the broad spectral shape of the XAS spectrum of MnSb induced by the mixing of different configurations. As for MnAlGe, the quite small orbital angular momentum may be due to the strong itinerancy of the Mn $3d$ electrons in spite of its more-than half filled feature as discussed above.

### C. Induced magnetic moments

The MCD spectrum of nonmagnetic elements can provide information on the induced magnetic moment resulting from the hybridization. For example, a clear MCD is reported in the S $2p$ XAS spectrum of ferromagnetic CoS$_2$, where the origin is mainly attributed to the exchange splitting resulting in the spin-dependent DOS of the unoccupied S $3d$ states.[26] Now we try to understand the observed Sb $3d$ MCD spectra of NiMnSb and Mn$_2$Sb by considering the spin-polarized DOS. The Sb $3d$ MCD is, however, in contrast to the S $2p$ MCD in CoS$_2$, in regard to the relative magnitude of MCD. Namely, the MCD of the Sb $3d$ state is up to 20% of the

XAS intensity after subtracting the background. This result suggests a remarkably spin-dependent occupation of the Sb $p$-like states in addition to the exchange splitting. The $d \rightarrow p$ transition probability is shown in Fig. 9. According to this figure, it is recognized that the up-spin electrons (down-spin electron) are more preferably excited with the $m = -1$ ($m = +1$) light at the $3d_{5/2}$ threshold, whereas the situation is just reversed at the $3d_{3/2}$ threshold. If we assume that the polarization of the Sb $5p$ state has the same sign as that of the Mn $3d$ state (down-spin states are more occupied), the MCD spectrum is expected to show the negative (positive) sign at the $3d_{5/2}$ ($3d_{3/2}$) threshold, inconsistent with our experimental results. Therefore the opposite spin-polarization of the Sb $5p$ states relative to the Mn $3d$ state [Mn(II) $3d$ state in Mn$_2$Sb] is confirmed in NiMnSb and Mn$_2$Sb. The band calculation also shows the antiparallel magnetic moment of Sb of about $-0.1 \mu_B$ in NiMnSb relative to the majority spin of the Mn $3d$ state of $+3.7 \mu_B$.[18,27] The calculation for Mn$_2$Sb, however, has predicted an induced magnetic moment of $+0.04 \mu_B$ on the Sb $5p$ state.[21] This theoretical result is inconsistent with our experimental result and requires reexamination.

The induced magnetic moment on Pt in PtMnSb has already been suggested in the previous section by the MCD signal in the Pt O$_3$ excitation around $h\nu = 58$ eV [Fig. 4(a)]. The XAS and MCD spectra in a wider energy region is shown as inset in Fig. 10. The sign of the MCD result also suggests that the magnetic moment of the Pt $5d$ orbital is parallel to the majority Mn $3d$ state. In the case of the Pt N$_{67}$ excitation spectrum, we can then expect the minus (plus) sign of the MCD spectrum in the N$_7$ (N$_6$) threshold region according to the $4f \rightarrow 5d$ dipole transition. The present experimental result has shown a ''W''-shaped line shape with a positive signal at the N$_7$ threshold which is followed by a negative MCD doublet and again a positive signal as shown in Fig. 10 in a strong contrast to the theoretical prediction. Recently, a very similar MCD spectrum has been observed in ferromagnetic CoPt$_3$.[28] The spectrum has been analyzed by considering a strong interference effect (Fano effect)[29] between the Coster-Krönig decay process $4f^{13}5d^{n+1} \rightarrow 4f^{14}5d^{n-1}\varepsilon 1$ of the $4f \rightarrow 5d$ absorption and the direct photoemission process $5d^n \rightarrow 5d^{n-1}\varepsilon 1$. The observed faint dip structure in the XAS spectrum and the ''W''-shaped MCD spectrum of PtMnSb are thus consistently interpreted by considering the above-mentioned Fano-type interference which often takes place in the resonant photoemission process.

### V. CONCLUSION

In summary, Mn, Ni, Sb, and Pt related core absorption and MCD spectra of some Heusler alloys (PtMnSb, NiMnSb, and Ni$_2$MnSb), NiAs-type MnSb and Cu$_2$Sb-type MnAlGe and Mn$_2$Sb have been measured. The nearly half-filled character of the Mn $3d$ states is revealed by the Mn $2p$ XAS and MCD spectra of the Heusler alloys, whereas the spectra of MnSb and MnAlGe show the more-than-half-filled features. In addition, the remarkable orbital angular momentum of the Mn $3d$ electrons is clarified for MnSb.

The Sb $3d$ core absorption MCD spectra of NiMnSb and

$Mn_2Sb$ have clearly revealed the induced magnetic moment on the Sb site and the importance of the hybridization between the Mn $3d$ and Sb $5p$ orbitals. The moment of Sb is found to be antiparallel to the Mn $3d$ moment in both NiMnSb and $Mn_2Sb$. The magnetic moment is also found on the Pt site in PtMnSb, where the moment of Pt is found to be parallel to that of the Mn $3d$ state.

---

*Present address: Synchrotron Radiation Laboratory, Institute for Solid State Physics, The University of Tokyo, Tokyo, Japan.

[1] K. Adachi and S. Ogawa, in Landolt-Börnstein New Series III/27a, edited by H. P. J. Wijn (Springer, Berlin, 1988), p. 385.

[2] P. G. van Engen, K. H. J. Buschow, R. Jongebreuer, and M. Erman, Appl. Phys. Lett. **42**, 202 (1983).

[3] T. Okita and Y. Makino, J. Phys. Soc. Jpn. **25**, 120 (1968).

[4] T. Hirata and S. Y. Koi, J. Phys. Soc. Jpn. **29**, 343 (1970).

[5] K. Adachi and S. Ogawa, in Ref. 1, p. 265.

[6] R. A. de Groot, F. M. Mueller, P. G. van Engen, and K. H. J. Buschow, J. Appl. Phys. **55**, 2151 (1984); R. A. de Groot, P. G. van Engen, and K. H. J. Buschow, J. Magn. Magn. Mater. **86**, 326 (1990).

[7] J. H. Wijingaard, C. Haas, and R. A. de Groot, Phys. Rev. B **40**, 9318 (1989).

[8] P. M. Oppeneer, V. N. Antonov, T. Kraft, H. Eschrig, A. N. Yaresko, and A. Ya. Perlov, Solid State Commun. **94**, 255 (1995).

[9] J. Kübler, A. R. Williams, and C. B. Sommers, Phys. Rev. B **28**, 1745 (1983).

[10] J. B. Goodenough, *Magnetism and the Chemical Bond* (Interscience, New York, 1963).

[11] Tu Chen, W. Stutius, J. W. Allen, and G. R. Steward, in *Magnetism and Magnetic Materials*, Proceedings of the 21st Annual Conference on Magnetism and Magnetic Materials, Philadelphia, 1975, edited by J. J. Becker, G. H. Lander, and J. J. Rhyne AIP Conf. Proc. No. **29** (AIP, New York, 1976), p. 532.

[12] J. W. Allen and J. C. Mikkelsen, Phys. Rev. B **15**, 2952 (1977).

[13] R. Coehoorn, C. Haas, and R. A. de Groot, Phys. Rev. B **31**, 1980 (1985).

[14] A. Kimura, S. Suga, H. Matsubara, T. Matsushita, Y. Saitoh, H. Daimon, T. Kaneko, and T. Kanomata, Solid State Commun. **81**, 707 (1992).

[15] U. Arp, F. Federmann, E. Källne, B. Sonntag, and S. L. Sorensen, J. Phys. B **25**, 3747 (1992).

[16] R. Bruhn, B. Sonntag, and H. W. Wolef, Phys. Lett. **69A**, 9 (1978).

[17] C. Haas and R. A. de Groot, in *Recent Advances in Magnetism of Transition Metal Compounds*, edited by A. Kotani and N. Suzuki (World Scientific, Singapore, 1993), p. 78.

[18] S. J. Youn and B. I. Min, Phys. Rev. B **51**, 10 436 (1995).

[19] B. T. Thole, R. D. Cowan, G. A. Sawatzky, J. Fink, and J. C. Fuggle, Phys. Rev. B **31**, 6856 (1985).

[20] K. Adachi and S. Ogawa, in Ref. 1, p. 148.

[21] M. Suzuki, M. Shirai, and K. Motizuki, J. Phys.: Condens. Matter **4**, L33 (1992); J. H. Wijingaard, C. Haas, and R. A. de Groot, Phys. Rev. B **45**, 5395 (1992).

[22] A. Kimura, S. Suga, T. Matsushita, T. Kaneko, and T. Kanomata, Solid State Commun. **85**, 901 (1993).

[23] A. Kimura, S. Suga, T. Matsushita, H. Daimon, T. Kaneko, and T. Kanomata, J. Phys. Soc. Jpn. **62**, 1624 (1993).

[24] M. Shirai and K. Motizuki, in *Recent Advances in Magnetism of Transition Metal Compounds*, edited by A. Kotani and N. Suzuki (World Scientific, Singapore, 1993), p. 67.

[25] P. Carra, B. T. Thole, M. Altarelli, and X. Wang, Phys. Rev. Lett. **70**, 694 (1993).

[26] T. Muro, T. Shishidou, F. Oda, T. Fukawa, H. Yamada, A. Kimura, S. Imada, S. Suga, S. Y. Park, T. Miyahara, and K. Sato, Phys. Rev. B **53**, 7055 (1996).

[27] E. Kulatov and I. I. Mazin, J. Phys.: Condens. Matter **2**, 343 (1990).

[28] T. Shishidou, S. Imada, T. Muro, F. Oda, A. Kimura, S. Suga, T. Miyahara, T. Kanomata, and T. Kaneko, Phys. Rev. B **55**, 3749 (1997).

[29] U. Fano, Phys. Rev. **124**, 1866 (1961).